# Effect of Activated Carbon Particle Size on Methylene Blue Adsorption Process in Textile Wastewater

**Akhmad Masykur Hadi Musthofa[1*], Mindriany Syafila[2], and Qomarudin Helmy[2]**

[1]*Department of Environmental Engineering, Institut Teknologi Bandung, Jl. Ganesha No. 10, Bandung 40132, West Java, Indonesia*

[2]*Water and Wastewater Engineering Research Group, Faculty of Civil and Environmental Engineering, Institut Teknologi Bandung, Jl. Ganesha No. 10, Bandung 40132, West Java, Indonesia*

* ***Corresponding author:***

*email: 25320307@mahasiswa.itb.ac.id*

*Received: December 7, 2022*
*Accepted: February 20, 2023*

**DOI:** 10.22146/ijc.79784

***Abstract:*** *Up to 60–70% of the total textile dyes produced are azo dyes. An example of azo dye is methylene blue, which is commonly used in dyeing wool, silk, and cotton. This substance possessed harmful effects on the environment. Therefore, the removal process is mandatory. The adsorption process is a common method for dye removal in wastewater. One innovation to increase adsorption efficiency even further is by reducing adsorbent particle size. To understand the effect of adsorbent particle size on the adsorption process, in this study, granular activated carbon (GAC) was pulverized into powder (PAC) and superfine powder (SPAC). Adsorbent characterizations, isotherm, kinetics, and thermodynamics tests were conducted. Based on this study, surface area, pore volume, and adsorption capacity were increased for smaller adsorbent particle sizes. Isotherm and kinetic analysis showed that there was no difference in the isotherm and kinetic models that applied to each activated carbon, but there was an increase in the isotherm and kinetic coefficient values at smaller particle sizes. Meanwhile, based on the thermodynamic test, there were differences in the dominant adsorption mechanism for each activated carbon. In GAC and SPAC, the dominant adsorption mechanism was electrostatic interactions, while in PAC was van der Waals forces.*

***Keywords:*** *activated carbon; adsorption; methylene blue; superfine powdered activated carbon*

## ■ INTRODUCTION

A textile company with an 8000 kg/day production capacity requires 1.6 million liters of water, with the dyeing process using about 16% of that amount. The wastewater from the dyeing process contributes around 10–15% of the total textile industry wastewater discharge [1]. The wastewater from the dyeing process contains high concentrations of dyes because some of the dyes do not bind to the textile fibers. The percentage of unbound dye concentrations varies from 1–50% depending on the type of dye used [2]. Because of this, the textile industry is considered to be the largest producer of dye effluents in the world, with a percentage of 54% of the total dye effluents produced [3].

It is estimated that there are 10,000 different types of textile dyes based on the color index. Among these various kinds of dyes, azo dyes are the most widely used dyes in the textile industry, reaching 60–70% of the total dyes produced [4]. An example of azo dye is methylene blue, which is commonly used in dyeing wool, silk, and cotton fabrics [5-6]. The release of wastewater containing azo dyes into the environment can reduce dissolved oxygen concentrations and degrade water quality. In addition, azo dyes also have acute toxicity, carcinogenic, and mutagenic effects on living things [7]. The dye concentration in the textile industry effluent varies from 10 to 250 mg/L [2].

Adsorption with activated carbon is a widely used dye-removal process. This process is considered to be fast, affordable, simple, does not produce sludge, has

high efficiency, is stable, and can be recycled [8-10]. To increase adsorption efficiency even further, reducing the particle size of activated carbon is one of the efforts which has been done [11]. Superfine powdered activated carbon (SPAC) is a result of reducing particle size to improve the adsorption process. SPAC is produced from the further reduction of powdered activated carbon (PAC) by a pulverization process using a bead mill, ball mill, or micro grinding to a size of < 1 μm. SPAC is considered to have advantages over PAC in terms of adsorption capacity and high rate of absorption kinetics [12-14].

The study about the effects of activated carbon particle size was limited because previously, it was believed that adsorption occurred in the internal pores of activated carbon, which does not depend on particle size [15]. This belief was later contradicted by some newer studies, which showed a significant effect of activated carbon particle size on adsorption capacities, especially in the adsorption of large molecular organic matters [16]. Although SPAC not always have higher adsorption capacity (depending on the adsorbate molecules), the kinetic rate of SPAC was always found to be superior compared to PAC [15,17-19]. Based on these findings, SPAC has a big potential to be used in the water/wastewater treatment process. Therefore, to understand the effect of particle size of activated carbon even further, this research not only analyzes the adsorption capacity and kinetics but also analyzes the thermodynamics of the adsorption process. In this study, the analysis was carried out on three types of activated carbon with different sizes, namely granular, powder, and superfine powdered.

## ■ EXPERIMENTAL SECTION

### Materials

The materials used in this study were deionized water, methylene blue dye (99% purity, Merck 115943 C.I.52015), and Jacobi-activated carbon AquaSorb 1000.

### Instrumentation

Several instruments used in the experimental phase of this study include mortar and pestle, laboratory glassware (beaker glass, Erlenmeyer flask, volumetric flask), high energy ball mill (Retsch planetary ball mill PM 400), Scanning Electron Microscope test instrumentation (SEM-EDX JEOL JSM-6510LA), Brunauer-Emmett-Teller test instrumentation (BET, Quantachrome Autosorb iQ ASiQwin-Automated Gas Sorption), Fourier transform Infrared Spectroscopy test instrumentation (Shimadzu FTIR Prestige 21), nanoparticle size analyzer (Horiba SZ-100), mechanical sieve shaker (Gilson SS-8R), jartest (VELP Scientifica JLT6), pH meter (ATC Pen Type PH-009), centrifuge (Hettich Rotofix 32 A 35° angle rotor 12-place), Visible light spectrophotometer (Thermo Scientific Genesys 30), heating and magnetic stirrer (Thermo Scientific Cimarec 2), and analytical scale (OHAUS PA224).

### Procedure

#### *Size reduction and activated carbon characterization*

The activated carbon used in this study was Jacobi Aquasorb 1000 which is a commercial granular activated carbon (GAC). The 20 g of Jacobi Aquasorb 1000 was mashed using a mortar and pestle for 20 min to become powder (PAC). Some of the PAC was further pulverized to become superfine powdered activated carbon (SPAC) using a high energy ball mill with a rotational speed of 350 rpm for 8 h. All activated carbons were then characterized physically and chemically. Physical characterizations consist of an analysis of particle size distribution (mechanical sieving and PSA), SEM, and BET tests. The particle size distribution of GAC and PAC was carried out using a mechanical sieving device, and the test for SPAC was carried out using a nanoparticle size analyzer at a scattering angle of 90°. The SEM test for GAC was performed at magnifications of 500, 1000, 2000, and 5000 times while the magnifications used for PAC and SPAC were 2000, 5000, 10000, and 20000 times. Meanwhile, the chemical characterizations of activated carbon were carried out by FTIR test at the wavelength of 400–4000 $cm^{-1}$ and point of zero charge test conducted according to Khalil et al. [20].

#### *Preliminary test of particle size effect on equilibrium and adsorption capacity*

This test was carried out by contacting different types of activated carbon (GAC, PAC, and SPAC) with

methylene blue artificial wastewater. Activated carbon as much as 1 g was contacted with 500 mL of methylene blue artificial wastewater at a concentration of 250 mg/L. The mixture was then stirred at a speed of 120 rpm to ensure there was sufficient contact between the adsorbent and the adsorbate [21]. Samples of PAC and SPAC mixture were then taken at a time range of 10, 20, 30, 60, 90, and 120 min to measure the concentration of dyes and COD [22]. Whereas in the GAC mixture, the sampling time was extended to 150, 180, 210, and 240 min to ensure equilibrium was reached.

After the test, PAC and SPAC were separated from the wastewater by centrifugation process with a force of 4.146 G for 5 and 20 min. The determination of color concentration was carried out by converting the color absorbance values using a visible spectrophotometer at a wavelength of 664 nm with a calibration curve [22-23]. Meanwhile, the determination of COD concentration was carried out using a method based on SNI 6989.2: 2019 about Spectrophotometric Closed Reflux COD Analysis.

### *Particle size effect on adsorption isotherms test*

Identification of activated carbon particle size effect on adsorption isotherms was carried out by contacting 1 g of GAC or PAC with 500 mL of methylene blue artificial wastewater at various dye concentrations 100, 125, 150, 175, and 200 mg/L. At the same time, the variations in dye concentration used in the identification of SPAC adsorption isotherms were 300, 350, 400, 450, and 500 mg/L. This mixture was then stirred with a stirring speed of 120 rpm for 120 min (PAC and SPAC) and 240 min (GAC). The determination of dye concentration variation and length of contact time was based on preliminary tests. The experimental data were then analyzed with non-linear equations of the isotherm model to find out the isotherm coefficient values using OriginPro2022b. Non-linear equations were used to minimize bias due to data transformation into linear equations. The obtained data then matched with Giles isotherm classification to determine the most suitable isotherm model and the adsorption mechanism for each activated carbon [24-26].

### *Particle size effect on adsorption kinetics test*

The adsorption kinetics test was carried out by contacting 1 g of activated carbon with 500 mL of methylene blue artificial wastewater at a dye concentration of 250 mg/L. The determination of duration for the adsorption kinetics test was based on preliminary test results. In the SPAC experiment, samples were taken every 4 min for 20 min; in the PAC experiment, samples were taken every 12 min for 60 min; and in the GAC experiment, samples were taken every 42 min for 210 min. Analysis of the kinetic coefficient values was carried out by matching the experimental data with the non-linear equations of the kinetic model using OriginPro2022b. If based on the isotherm analysis, the adsorption process dominated by chemisorption, the kinetic test data will be matched with pseudo-second-order model. Meanwhile, if the dominant mechanism in adsorption process is physisorption, the kinetics test data will be matched with pseudo-first-order and intraparticle diffusion model. To determine which model is more suitable, error analysis between the value of adsorption capacity at certain time ($q_t$) based on model and $q_t$ value based on experiment will be conducted. The error analysis consists of sum of square error (SSE), average relative error (ARE), hybrid fractional error function (HYBRID), and The Marquardt's percent standard deviation (MPSED). The equations for each error analysis can be seen in Eq. (1) through Eq. (4) as follows [24-26].

$$\mathrm{SSE} = \sum \left( q_{t,\mathrm{cal}} - q_{t,\mathrm{exp}} \right)^2 \tag{1}$$

$$\mathrm{ARE} = \frac{1}{\mathrm{N}} \sum \left| \frac{q_{t,\mathrm{cal}} - q_{t,\mathrm{exp}}}{q_{t,\mathrm{exp}}} \right| \times 100 \tag{2}$$

$$\mathrm{HYBRID} = \frac{1}{\mathrm{N-P}} \sum \frac{\left( q_{t,\mathrm{cal}} - q_{t,\mathrm{exp}} \right)^2}{q_{t,\mathrm{exp}}} \times 100 \tag{3}$$

$$\mathrm{MPSED} = \sqrt{\frac{\sum \left( \left( q_{t,\mathrm{exp}} - q_{t,\mathrm{cal}} \right) / q_{t,\mathrm{exp}} \right)^2}{\mathrm{N-P}}} \times 100 \tag{4}$$

where $q_{t,cal}$ is the adsorption capacity at certain time (t) based on calculation from each model (mg/g), $q_{t,exp}$ is the adsorption capacity at certain time (t) based on the

experiment (mg/g), N is the number of data, and P is the degree of freedom.

***Particle size effect on adsorption thermodynamics test***

The thermodynamic analysis was carried out by varying the temperature of the adsorption system to 25, 35, 45, and 55 °C. From the obtained data, the maximum adsorption capacity was determined to calculate the value of $K_e$ (adsorption thermodynamic constant) with Eq. (5) as follows:

$$K_e = \frac{q_e/q_m}{(1-q_e/q_m)C_e/C_0} \quad (5)$$

where $q_e$ is the adsorption capacity at equilibrium (mol/g), $q_m$ is the maximum adsorption capacity (mol/g), $C_e$ is the adsorbate concentration at equilibrium (mol/L), and $C_0$ is the molar concentration of the standard reference solution (assumed to be 1 mol/L).

After that, a Van't Hoff curve can be constructed, which is a plot of $\ln(K_e)$ to 1/T. The values of ΔH° (standard enthalpy change) and ΔS° (standard entropy change) can be identified based on the slope and intercept of the Van't Hoff curve [25,27].

## ■ RESULTS AND DISCUSSION

FTIR test was performed on PAC and SPAC. The results of the GAC FTIR test were considered to be the same as PAC because they came from the same material source, namely Jacobi Aquasorb 1000. Meanwhile, the SPAC test was carried out to determine whether the pulverization process with a high-energy ball mill caused changes in functional groups on the surface of the activated carbon. The FTIR test results, as shown in Fig. 1 indicated that SPAC and PAC produced the same peak at wavelengths of 3429.43 and 1568.13 $cm^{-1}$, which indicated the presence of a functional group in the form of a hydroxyl group (-OH) and an aromatic bond in the form of C=C. However, the SPAC FTIR test showed a lower transmission value (%T) at a wavelength of 3429.43 $cm^{-1}$. A lower %T value indicates a greater number of functional groups on the activated carbon surface. Therefore, it can be concluded that the pulverization process with a ball mill did not cause a change in the type of functional groups but increased the number of functional groups available on the activated carbon surface. Apart from these two wavelengths, the peak also occurs at a wavelength of 460.99; 796.60; 1091.71 $cm^{-1}$, which probably indicates the presence of functional groups of C-O and C-C, C-H, and C-O-C, which are commonly found in ether, ester or phenol groups [20,28].

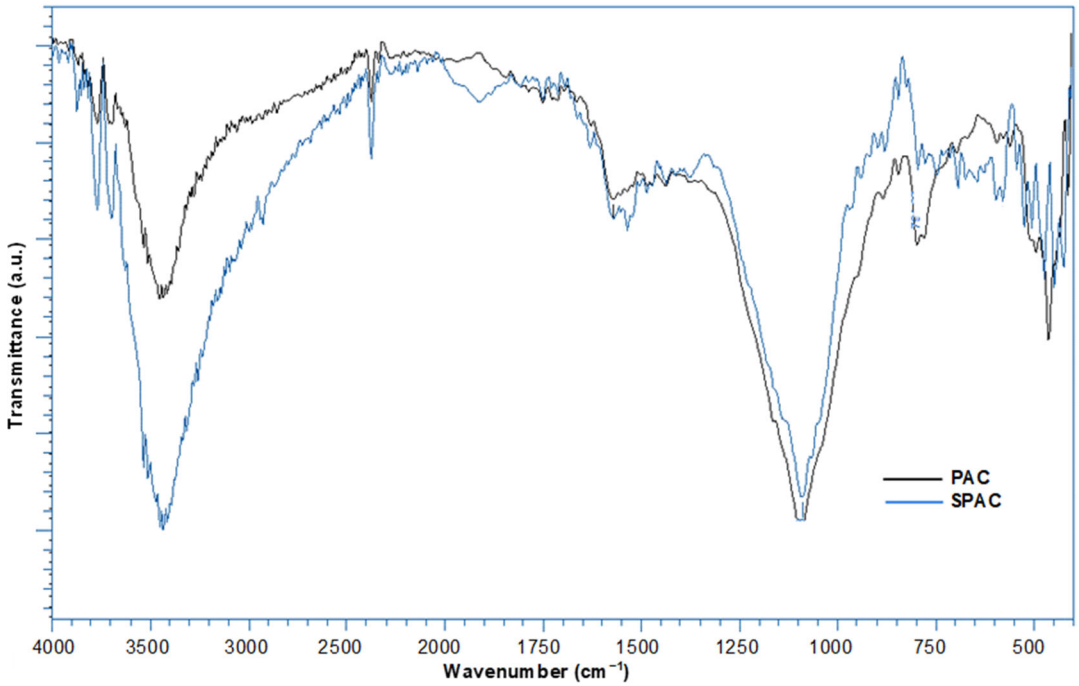


**Fig 1.** FTIR test results of PAC and SPAC

Another chemical characterization test of adsorbent, which was zero point of discharge, showed different results on each activated carbon. The $pH_{PZC}$ value of GAC was 6.65, while the $pH_{PZC}$ values of PAC and SPAC were 6.75 and 7.00, as shown in Fig. 2. This finding showed that activated carbon was more alkaline at smaller particle sizes. These results are different from previous research [17,29]. In those studies, the $pH_{PZC}$ values decreased at smaller particle sizes, indicating a more acidic nature. This difference can possibly be caused by a different source of activated carbon used. In the previous study, activated carbon was made from wood, coconut shell, and lignite coal. Meanwhile, the activated carbon used in this study was made from bituminous coal.

Based on the mechanical sieving test, GAC particle size ranged from 0.42–2.00 mm with a $d_{50}$ of 0.58 mm. The dominant GAC particle size was 1.18 and 2.00 mm, with occurrence frequencies reaching 71.02 and 22.40%. The particle size of PAC ranges from 0.053–0.42 mm with a $d_{50}$ of 0.108 mm. The dominant PAC particle size was 0.42 and 0.149 mm, with occurrence frequencies of 28.68 and 36.13%. Meanwhile, based on the nanoparticle size analysis test, the particle size of SPAC ranged from 246.98–4622.81 nm with a $d_{50}$ of 550 nm and an average diameter size of 704.93 nm. The dominant particle size was in the range of 315.27–513.71 nm with occurrence frequencies ranging from 4 to 13% and 1541.04–2511.05 nm with occurrence frequencies ranging from 5 to 6%. The average size of the SPAC in this study complied with the applicable requirement which is smaller than 1 µm. The detailed results of mechanical sieving tests and particle size analysis can be seen in Fig. 3, 4, and 5.

The SEM test results on GAC with the magnification of 500, 1000, 2000, and 5000 times are shown in Fig. 6. Based on that figure, the GAC surface was corrugated and porous. However, the pores formed were not uniform, and some of the pore openings were covered with smaller particles. Porous surfaces were also identified in the PAC SEM test results with magnifications of 2000, 5000, 10000, and 20000 times as seen in Fig. 7. Pores on the PAC surface were seen more clearly than on the GAC surface. This can be caused by the opening of small diameter pores to become larger due to the pulverization process [30]. Meanwhile, the SEM test results on SPAC with the magnification of 2000, 5000, 10000, and 20000×, which can be seen in Fig. 8, showed that the particle size of the adsorbent was smaller than the previous two types of adsorbents. This is in accordance with the results of the particle size analysis test that has been described previously.

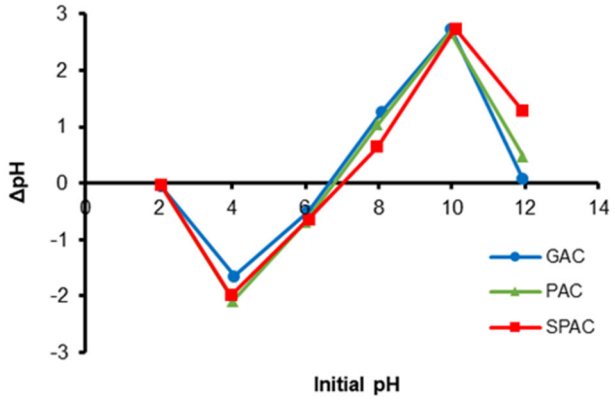


**Fig 2.** Point of zero charge test result

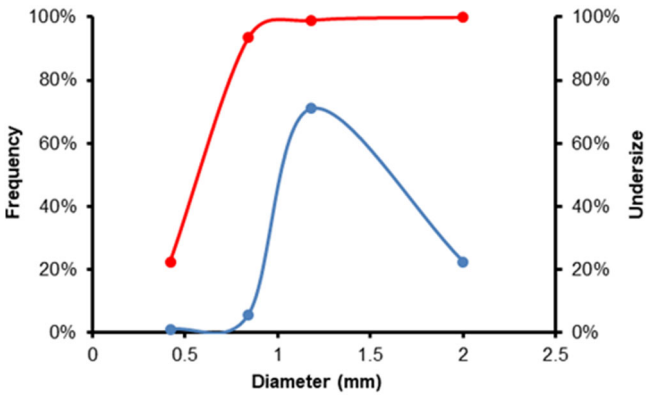


**Fig 3.** Particle size distribution of GAC

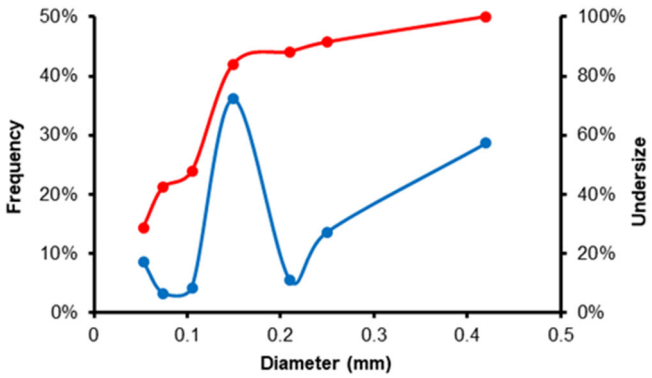


**Fig 4.** Particle size distribution of PAC

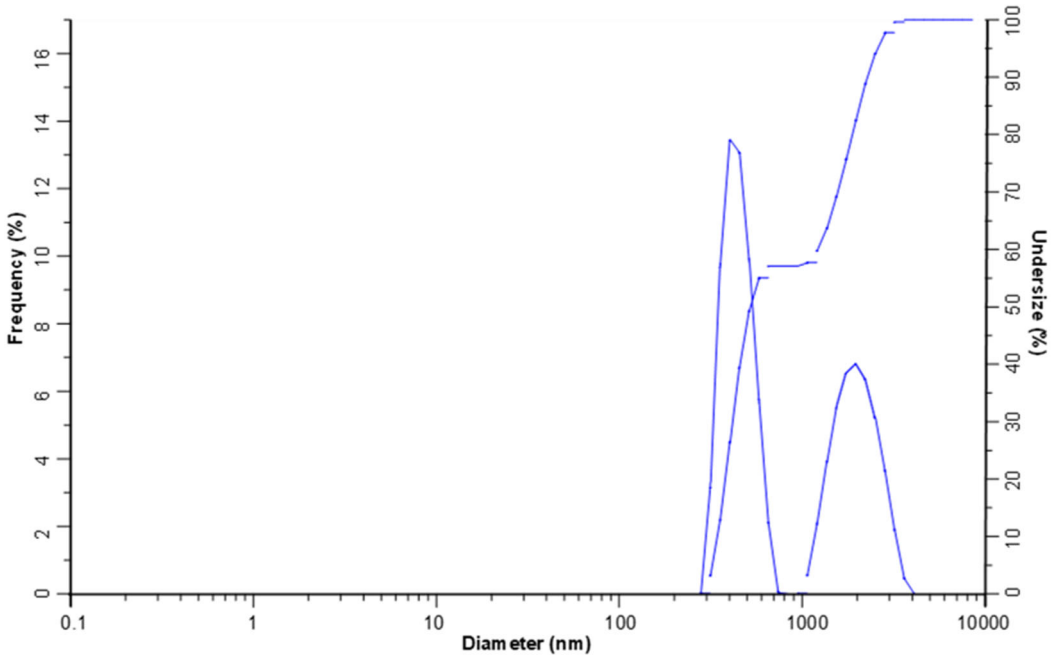


**Fig 5.** Particle size distribution of SPAC

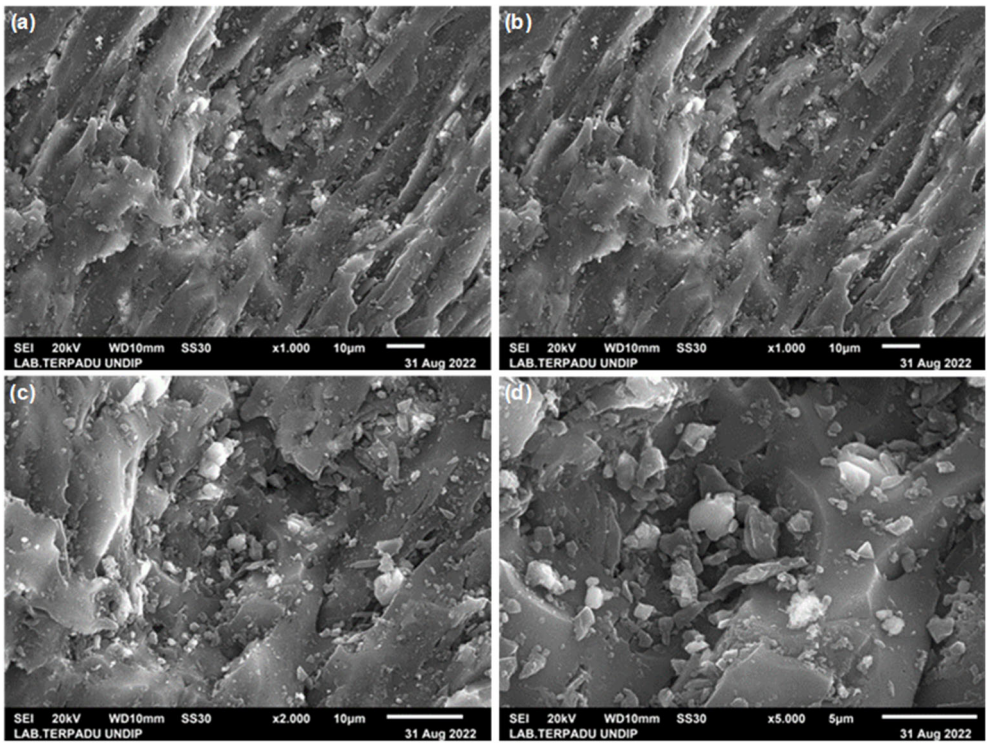


**Fig 6.** SEM test results of GAC with magnification of (a) 500×, (b) 1000×, (c) 2000×, and (d) 5000×

Based on BET tests, size reduction of activated carbon from GAC to PAC and SPAC caused an increase in total pore volume and surface area of activated carbon. The total pore volume increased from 0.4576 $cm^3/g$ (GAC) to 0.4618 $cm^3/g$ (PAC) and 0.4743 $cm^3/g$ (SPAC). This increase in pore volume can be caused by the formation of spaces between particles due to the pulverizing process, which is then measured as pores [29].

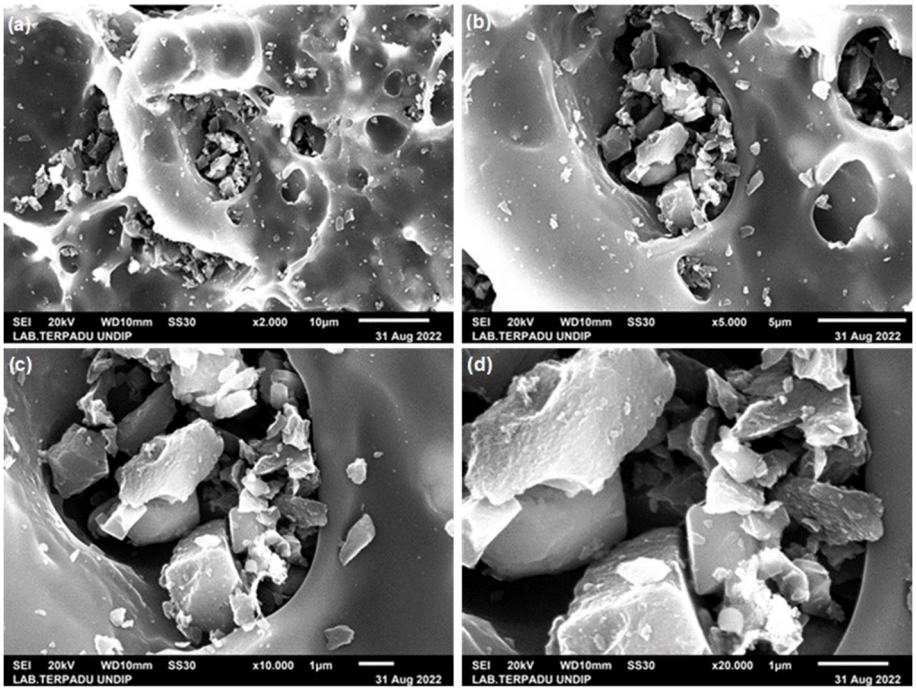


**Fig 7.** SEM test results of PAC with magnification of (a) 2000×, (b) 5000×, (c) 10000×, and (d) 20000×

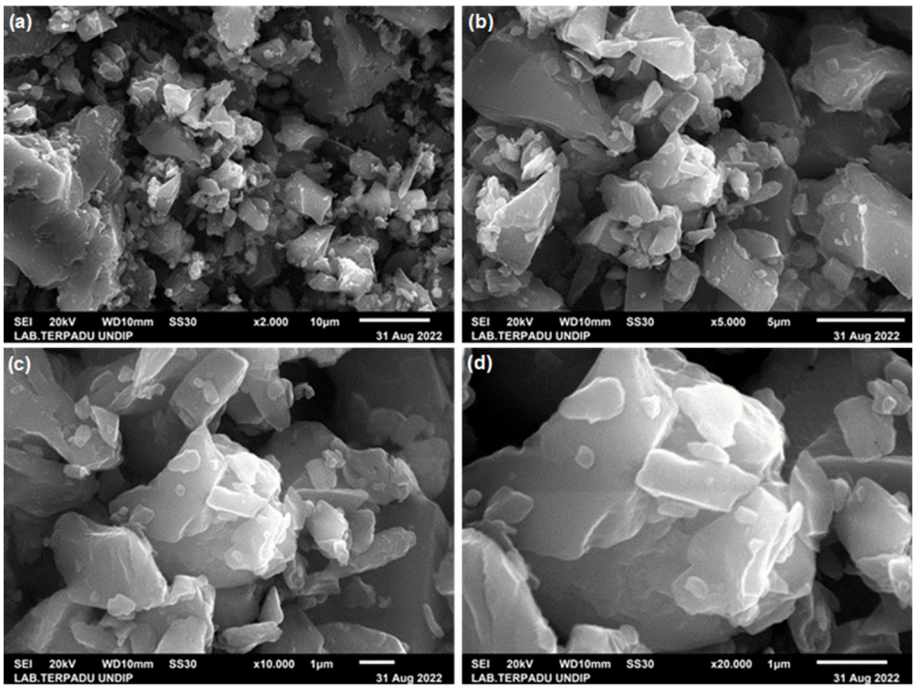


**Fig 8.** SEM test results of SPAC with magnification of (a) 2000×, (b) 5000×, (c) 10000×, and (d) 20000×

These results were in accordance with previous research, which stated that the activated carbon particle size change did not cause a substantial change in pore structure [12,31]. Meanwhile, the surface area of activated carbon increased from 776.439 $m^2/g$ (GAC) to 787.443 $m^2/g$ (PAC) and 790.478 $m^2/g$ (SPAC). This increase was due to a reduction of particle size and pore widening of activated carbon. But the escalation of surface area in smaller particle size was not as significantly different as particle size. This can be caused by the disappearance of

some surface area available in the parent material, such as pore channels, due to the pulverization process [29-30].

## Preliminary Tests

Preliminary test results showed that activated carbon was effective at removing the dye in methylene blue artificial wastewater. SPAC had the highest dye adsorption capacity compared to PAC and GAC. The dye adsorption capacities of SPAC ranged from 112.57–122.21 mg/g, while the dye adsorption capacities of PAC and GAC ranged from 34.67–60.96 mg/g and 4.34–16.66 mg/g. Reduction in dye concentration was also followed by a decrease in COD concentration. The COD adsorption capacities of SPAC ranged from 158.97–171.32 mg/g, while the COD adsorption capacities of PAC and GAC ranged from 39.64–55.61 mg/g and 9.91–22.99 mg/g. The escalation in adsorption capacity was mostly due to the increase of activated carbon's surface area rather than the increase in pores volume [18]. Structural pore changes due to the pulverizations process were not large. The increase in pore volume was only 0.0042 (GAC to PAC) and 0.0167 $cm^3/g$ (GAC to SPAC). But the increase in adsorption capacity can be explained based on the shell adsorption model (SAM). Based on SAM, more adsorbate is adsorbed on the outside (shell) of a particle if the radius of the activated carbon particle is smaller than the diffusion penetration depth of a particle whose value depends on the type of adsorbent and adsorbate. Because the outer surface area of the particles increases as the particle size decreases, the adsorption capacity increases [14].

## Particle Size Effect on Adsorption Isotherms Test

The isotherm test results on each activated carbon can be seen in Fig. 9. Based on the Giles isotherm classification, the methylene blue adsorption process on each activated carbon followed the "High-Affinity Isotherm". This is because the $q_e$ value is always greater than zero, even though the adsorbate concentration is close to zero. This type of isotherm generally occurs in adsorbates with large molecular sizes, such as polymers. This isotherm indicates the adsorption process occurs chemically (chemisorption) or adsorption by electrostatic forces 25].

Although each adsorption process followed a high-affinity isotherm, the adsorption process for each activated carbon was in a different subclass. The methylene blue adsorption process using GAC followed the mx subclass, while PAC and SPAC followed subclasses 4 and 2. The mx subclass was characterized by a decrease in adsorption capacity when the adsorbate concentration was increased. This decrease in adsorption capacity occurs because the interaction between the adsorbate molecules is stronger than the interaction between the adsorbate and the adsorbent. Subclass 4 is characterized by the presence of two lines with a gentle slope connected by a line with a steeper slope. This indicates the formation of a new active surface which can be caused by the reorientation of the adsorbed molecules from horizontal to vertical, which

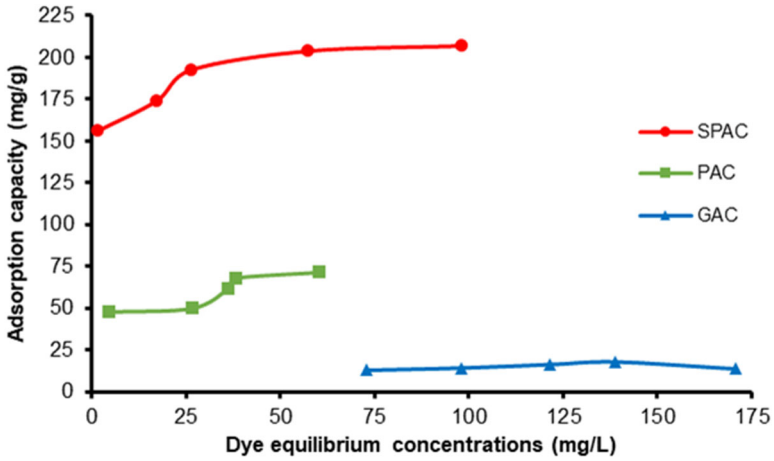


**Fig 9.** Isotherm graph

allows more adsorbate particles to be adsorbed. While subclass 2 is characterized by the appearance of longitudinal horizontal lines caused by the absence of intramolecular interactions of the adsorbate. Since there is no intramolecular interaction of the adsorbate, the adsorption process is monolayer [25]. All of these isotherm subclasses indicate a monolayer adsorption process. Therefore, the data obtained from the experiment were matched with the Langmuir isotherm to determine the value of the coefficient ($K_L$) and maximum adsorption capacity ($q_m$) using OriginPro2022b. $q_m$ and $K_L$ values can be seen in Table 1.

The maximum adsorption capacity and Langmuir coefficient ($K_L$) increased in the adsorbent with the smaller particle size. An increase in $K_l$ value indicates a stronger interaction between the adsorbent and the adsorbate on the smaller activated carbon particles [32]. The increase in maximum adsorption capacity for adsorbents with smaller particle sizes also occurred in previous research [15,29]. According to Ando et al. [31] adsorption capacity of activated carbon for certain adsorbate depends on adsorbent particle size. The dependence of adsorption capacity on activated carbon particle size might be associated with high-molecular mass of adsorbate and adsorbate characteristics. Moreover, the properties of activated carbon can also affect the adsorption capacity in smaller particle sizes.

## Particle Size Effect on Adsorption Kinetics Test

Based on isotherm analysis, the adsorption process of methylene blue on all activated carbon was caused by electrostatic forces. This will be further proven in thermodynamic tests to determine the enthalpy value of the adsorption process. Because the adsorption process was caused by electrostatic forces, the adsorption process was considered physisorption. Several kinetic models that can be used to describe the kinetics of the physisorption process are pseudo-first order and intraparticle diffusion models [33-34]. Therefore, the experimental data were analyzed with both models using OriginPro 2022b. From these two models, one model was then selected based on the lowest sum of square error (SSE), average relative error (ARE), hybrid fractional error function (HYBRID), and The Marquardt's percent standard deviation (MPSED) [24,35]. Analysis of the kinetic parameters using OriginPro2022b produced kinetic parameters of the pseudo-first-order and intraparticle diffusion models as seen in Table 2 and 3.

Error analysis to compare the suitability of each model to the experimental data can be seen in Table 4. Based on Table 4, the pseudo-first-order kinetic model had smaller error values for all types of activated carbon compared to the intraparticle diffusion model. This indicates that the first-order pseudo model was more

**Table 1.** Langmuir Isotherm Coefficients

| Adsorbent types | $q_m$ (mg/g) | $K_L$ (L/mg) |
|---|---|---|
| GAC | 27.72505 ± 3.49558 | 0.01156 ± 0.00329 |
| PAC | 66.46779 ± 5.81396 | 0.51107 ± 0.38549 |
| SPAC | 197.70408 ± 7.1626 | 2.28743 ± 1.00784 |

**Table 2.** Pseudo-first-order kinetic parameters

| Adsorbent types | $K_1$ ($min^{-1}$) | $q_e$ (mg/g) |
|---|---|---|
| GAC | 0.01472 ± 0.00129 | 24.15746 ± 0.74313 |
| PAC | 0.11407 ± 0.04308 | 41.66993 ± 2.97193 |
| SPAC | 1.13446 ± 0.03338 | 119.82991 ± 0.07587 |

**Table 3.** Intraparticle diffusion kinetic parameters

| Adsorbent types | Ki ($mg/g.min^{-0.5}$) | $C_i$ (mg/g) |
|---|---|---|
| GAC | 1.47001 ± 0.11054 | 2.85518 ± 1.23684 |
| PAC | 2.59757 ± 1.26843 | 35.53882 ± 7.6106 |
| SPAC | 0.53902 ± 0.15386 | 117.76349 ± 0.53299 |

**Table 4.** Error values of kinetic models

| Adsorbent types | Time (min) | $q_{t,exp}$ (mg/g) | Pseudo-first-order | | | | | Intraparticle diffusion | | | | |
|---|---|---|---|---|---|---|---|---|---|---|---|---|
| | | | $q_t$ (mg/g) | SSE | ARE | HYBRID | MPSED | $q_t$ (mg/g) | SSE | ARE | HYBRID | MPSED |
| GAC | 42 | 11.84 | 11.14 | | | | | 12.38 | | | | |
| | 84 | 16.63 | 17.14 | | | | | 16.33 | | | | |
| | 126 | 20.19 | 20.38 | 1.148 | 2.709 | 2.492 | 4.178 | 19.36 | 1.435 | 2.607 | 2.657 | 3.982 |
| | 164 | 21.68 | 22.00 | | | | | 21.68 | | | | |
| | 210 | 23.56 | 23.06 | | | | | 24.16 | | | | |
| PAC | 12 | 33.42 | 31.07 | | | | | 44.54 | | | | |
| | 24 | 35.83 | 38.97 | | | | | 48.26 | | | | |
| | 36 | 36.60 | 40.98 | 70.661 | 8.307 | 57.459 | 11.961 | 51.12 | 710.742 | 31.017 | 632.012 | 41.245 |
| | 48 | 41.01 | 41.50 | | | | | 53.54 | | | | |
| | 60 | 47.61 | 41.63 | | | | | 55.66 | | | | |
| SPAC | 4 | 118.55 | 118.55 | | | | | 118.84 | | | | |
| | 8 | 119.60 | 119.82 | | | | | 119.29 | | | | |
| | 12 | 119.84 | 119.83 | 0.068 | 0.071 | 0.019 | 0.126 | 119.63 | 0.269 | 0.176 | 0.075 | 0.251 |
| | 16 | 119.89 | 119.83 | | | | | 119.92 | | | | |
| | 20 | 119.97 | 119.83 | | | | | 120.17 | | | | |

**Table 5.** Adsorption thermodynamics parameters

| Temp (K) | $C_e$ (mol/L) | $q_e$ (mol/g) | $q_m$ (mg/g) | $K_e$ | ΔG° (KJ/mol) | ΔH° (KJ/mol) | ΔS° (J/mol.K) |
|---|---|---|---|---|---|---|---|
| GAC | | | | | | | |
| 298 | 0.000228 | 0.000041 | 27.73 | 3886.50 | -20.48 | 59.92 | 272.35 |
| 308 | 0.000169 | 0.000064 | 28.77 | 14965.52 | -24.62 | | |
| 318 | 0.000128 | 0.000092 | 35.52 | 38167.25 | -27.89 | | |
| 328 | 0.000123 | 0.000097 | 38.87 | 32221.93 | -28.31 | | |
| PAC | | | | | | | |
| 298 | 0.000014 | 0.000149 | 66.47 | 187063.39 | -30.08 | 14.68 | 150.94 |
| 308 | 0.000007 | 0.000150 | 72.91 | 288742.62 | -32.20 | | |
| 318 | 0.000006 | 0.000151 | 74.63 | 294613.25 | -33.30 | | |
| 328 | 0.000006 | 0.000160 | 77.67 | 337172.66 | -34.71 | | |
| SPAC | | | | | | | |
| 298 | 0.000005 | 0.000488 | 197.70 | 780186.08 | -33.61 | 58.92 | 309.46 |
| 308 | 0.000002 | 0.000445 | 201.94 | 1571975.09 | -36.54 | | |
| 318 | 0.000001 | 0.000463 | 205.83 | 1798797.87 | -38.08 | | |
| 328 | 0.000000 | 0.000468 | 207.92 | 8525412.86 | -43.52 | | |

suitable for describing the adsorption mechanism that occurred. In addition, based on Table 2, the value of the adsorption kinetics coefficient increased on activated carbon with a smaller particle size. This indicates a faster adsorption process on SPAC compared to PAC or GAC. An increase in the adsorption rate on the smaller activated carbon particles also occurred in previous research [17,19].

## Particle Size Effect on Adsorption Thermodynamics Test

The results of the thermodynamic test on each activated carbon can be seen in Table 5. Based on Table 5, the change in Gibbs free energy (ΔG°) was negative. This indicates that the methylene blue adsorption process using activated carbon was spontaneous and favorable. The increasingly negative ΔG° value indicates

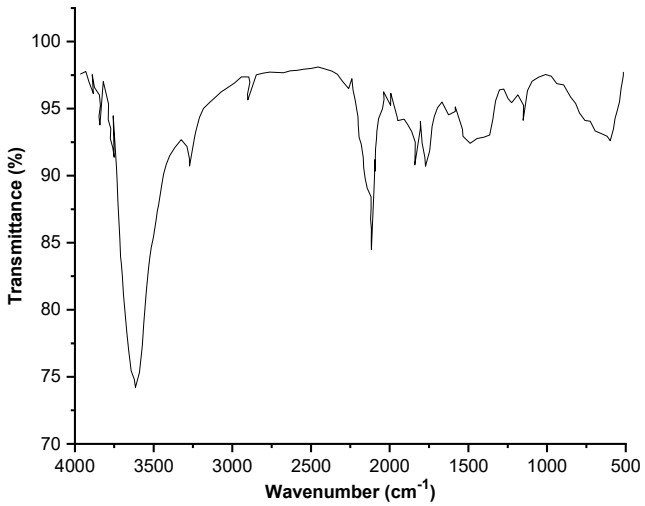


**Fig 10.** FTIR test results of MB solution before adsorption process

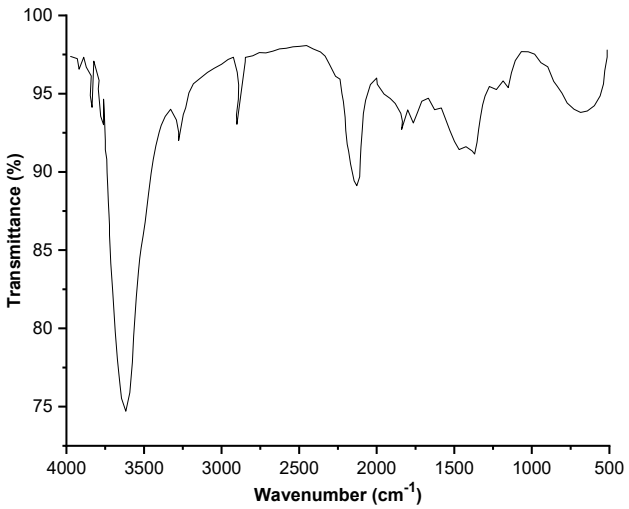


**Fig 11.** FTIR test results of MB solution after adsorption process

that the adsorption process was better and more spontaneous on the smaller activated carbon particle size and at higher temperatures [25].

Unlike the ΔG° values, the ΔH°, and ΔS° values were positive for all activated carbons. A positive ΔH° value indicates the adsorption process was endothermic. This is proven by the increased adsorption capacity at higher temperatures. Meanwhile, a positive ΔS° value indicates increased randomness at the interface of adsorbent-adsorbate and a good affinity of adsorbent to adsorbate [25]. The value of ΔH° can also be used to determine the adsorption mechanism that occurred. The value of ΔH° at PAC, which was less than 20 KJ/mol indicates physisorption was dominated by van der Waals forces interactions. Meanwhile, the ΔH° values of GAC and SPAC which were in the range of 20–80 KJ/mol indicate physisorption was dominated by electrostatic interactions.

These adsorption mechanisms were supported by FTIR test results on methylene blue artificial wastewater before and after the adsorption process (Fig. 10 and 11). Before the adsorption process, methylene blue artificial wastewater showed peaks in the functional group region ($\lambda > 1500$ cm$^{-1}$) at the wavelength of 3429.43; 2924.09; 2856.58; and 1602.85 cm$^{-1}$. These peaks indicated the presence of hydroxyl (OH-), methylene ($CH_2$), methyl ether (O-$CH_3$), and C=C functional groups. Meanwhile in fingerprint region ($\lambda < 1500$ cm$^{-1}$) peaks were formed at wavelength of 1492.90; 1442.75; 1396.46; 1350.17; 1247.94; 1176.58; 1141.86; and 1041.56 cm$^{-1}$. These peaks could be formed because of the presence of aromatic bonds of (C=C-C), methyl ($CH_3$), tri-methyl, methine (=CH-), aromatic ether, secondary amine (C-N), cyclic ether, and cyclohexane ring [36]. After the adsorption process, peaks in the functional group region remain unchanged. But, in the fingerprint region, some peaks disappeared at wavelength 1492.90; 1442.75; 1247.94; and 1176.58 cm$^{-1}$.

The disappearance of some functional groups could be caused by several interactions: 1) π-π interactions between the aromatic functional groups on the surface of the adsorbent and aromatic bonds (C=C-C), aromatic ethers, and other benzenic rings of methylene blue, 2) Electrostatic interactions between the negatively charged functional groups on the surface of the adsorbent and the positively charged methylene blue molecules (cations), 3) The hydrogen bond between the nitrogen (N) on the methylene blue molecule and functional groups containing oxygen, such as hydroxyl (OH-) on the surface of activated carbon [6,20,37].

The schematic mechanisms of the methylene blue adsorption process can be seen in Fig. 12.

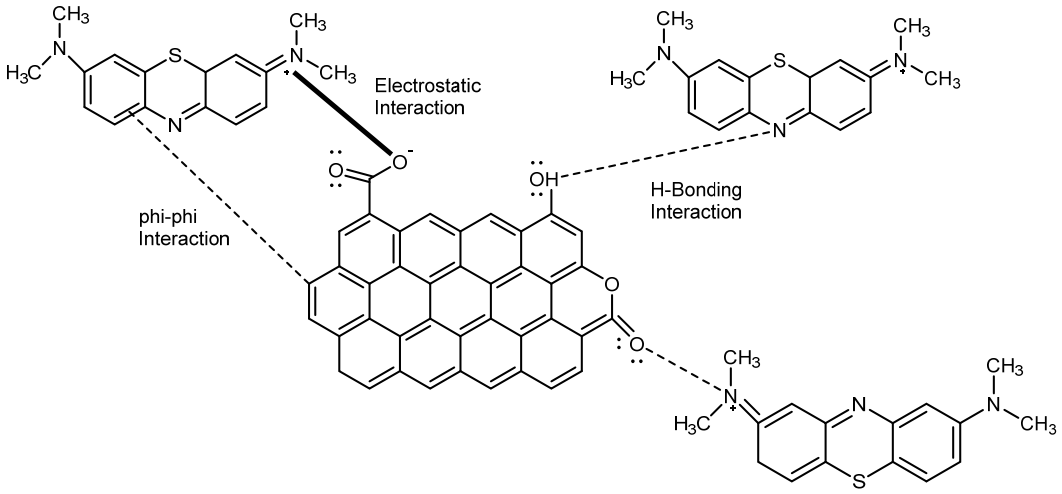


**Fig 12.** Scheme of adsorption interactions of MB and activated carbon

## ■ CONCLUSION

The chemical characterization of activated carbon showed that the pulverization process could change the $pH_{pzc}$ to be more alkaline and increase the number of functional groups present on the surface of the activated carbon but did not change the type of functional groups available. At the same time, the physical characterization showed that there were differences in particle size distribution in GAC, PAC, and SPAC. The pulverization process also caused an increase in the surface area and pore volume of activated carbon. Based on isotherm and kinetic analysis, particle size variations did not change the type of isotherm and kinetics model that applied to the adsorption process, but it caused an increase in maximum adsorption capacity, Langmuir coefficient, and kinetics coefficient in smaller particle sizes. The thermodynamic test showed that the adsorption process took place more spontaneously and more favorably at the smaller particle size, and there was a difference in the dominant mechanism that caused the adsorption process in different particle sizes of activated carbon based on $\Delta H°$ values. The dominant adsorption mechanism on GAC and SPAC was electrostatic interaction, while on PAC was van der Waals forces. Based on these results, SPAC has good potential to be used in the water/wastewater treatment process, especially in the tertiary process, to remove recalcitrant pollutants such as hydrocarbons, pesticides, and textile dyes.

## ■ AUTHOR CONTRIBUTIONS

Akhmad Masykur Hadi Musthofa conducted the experiments, calculations, and wrote the manuscript. Mindriany Syafila and Qomarudin Helmy reviewed the methodology and manuscript. All authors agreed to the final version of this manuscript.

## ■ REFERENCES

[1] Kant, R., 2012, Textile dyeing industry an environmental hazard, *Nat. Sci.*, 4 (1), 22–26.

[2] Ghaly, A.E., Ananthashankar, R., Alhattab, M., and Ramakrishna, V.V., 2013, Production, characterization and treatment of textile effluents: A critical review, *J. Chem. Eng. Process Technol.*, 5 (1), 1000182.

[3] Velusamy, S., Roy, A., Sundaram, S., and Kumar Mallick, T., 2021, A review on heavy metal ions and containing dyes removal through graphene oxide-based adsorption strategies for textile wastewater treatment, *Chem. Rec.*, 21 (7), 1570–1610.

[4] Balapure, K., Bhatt, N., and Madamwar, D., 2015, Mineralization of reactive azo dyes present in simulated textile waste water using down flow microaerophilic fixed film bioreactor, *Bioresour. Technol.*, 175, 1–7.

[5] Fatkhasari, Y., Rouf, N.A., Ermadayanti, W.A., Kurniawan, R.Y., and Bagastyo, A.Y., 2019, Synthesis of $TiO_2$/zeolite-A composite for the

removal of methylene blue on direct sunlight, *Jurnal Teknik ITS*, 8 (2), 115–120.

[6] Giraldo, S., Robles, I., Godínez, L.A., Acelas, N., and Flórez, E., 2021, Experimental and theoretical insights on methylene blue removal from wastewater using an adsorbent obtained from the residues of the orange industry, *Molecules*, 26 (15), 4555.

[7] Saratale, R.G., Saratale, G.D., Chang, J.S., and Govindwar, S.P., 2011, Bacterial decolorization and degradation of azo dyes: A review, *J. Taiwan Inst. Chem. Eng.*, 42 (1), 138–157.

[8] Dutta, S., Gupta, B., Srivastava, S.K., and Gupta, A.K., 2021, Recent advances on the removal of dyes from wastewater using various adsorbents: A critical review, *Mater. Adv.*, 2 (14), 4497–4531.

[9] Sultana, M., Rownok, M.H., Sabrin, M., Rahaman, M.H., and Alam, S.M.N., 2022, A review on experimental chemically modified activated carbon to enhance dye and heavy metals adsorption, *Cleaner Eng. Technol.*, 6, 100382.

[10] Zhang, Z., Xu, L., Liu, Y., Feng, R., Zou, T., Zhang, Y., Kang, Y., and Zhou, P., 2021, Efficient removal of methylene blue using the mesoporous activated carbon obtained from mangosteen peel wastes: Kinetic, equilibrium, and thermodynamic studies, *Microporous Mesoporous Mater.*, 315, 110904.

[11] Sun, X., Ma, L., Ye, G., Wu, L., Li, J., Xu, H., and Huang, G., 2021, Phenol adsorption kinetics and isotherms on coal: Effect of particle size, *Energy Sources, Part A*, 43 (4), 461–474.

[12] Partlan, E., 2017, Superfine Powdered Activated Carbon (S-PAC) Coupled with Microfiltration for the Removal of Trace Organics in Drinking Water Treatment, *Dissertation*, Clemson University, South Carolina.

[13] Takaesu, H., Matsui, Y., Nishimura, Y., Matsushita, T., and Shirasaki, N., 2019, Micro-milling super-fine powdered activated carbon decreases adsorption capacity by introducing oxygen/hydrogen-containing functional groups on carbon surface from water, *Water Res.*, 155, 66–75.

[14] Pan, L., Nishimura, Y., Takaesu, H., Matsui, Y., Matsushita, T., and Shirasaki, N., 2017, Effects of decreasing activated carbon particle diameter from 30 μm to 140 nm on equilibrium adsorption capacity, *Water Res.*, 124, 425–434.

[15] Matsui, Y., Nakao, S., Sakamoto, A., Taniguchi, T., Pan, L., Matsushita, T., and Shirasaki, N., 2015, Adsorption capacities of activated carbons for geosmin and 2-methylisoborneol vary with activated carbon particle size: Effects of adsorbent and adsorbate characteristics, *Water Res.*, 85, 95–102.

[16] Shi, B., Fang, L., Li, Z., and Wang, D., 2014, Adsorption behavior of DOM by PACs with different particle sizes, *CLEAN – Soil, Air, Water*, 42 (10), 1363–1369.

[17] Partlan, E., Ren, Y., Apul, O.G., Ladner, D.A., and Karanfil, T., 2020, Adsorption kinetics of synthetic organic contaminants onto superfine powdered activated carbon, *Chemosphere*, 253, 126628.

[18] Matsui, Y., Ando, N., Yoshida, T., Kurotobi, R., Matsushita, T., and Ohno, K., 2011, Modeling high adsorption capacity and kinetics of organic macromolecules on super-powdered activated carbon, *Water Res.*, 45 (4), 1720–1728.

[19] Bonvin, F., Jost, L., Randin, L., Bonvin, E., and Kohn, T., 2016, Super-fine powdered activated carbon (SPAC) for efficient removal of micropollutants from wastewater treatment plant effluent, *Water Res.*, 90, 90–99.

[20] Khalil, K.M.S., Elhamdy, W.A., Mohammed, K.M.H., and Said, A.E.A.A., 2022, Nanostructured P-doped activated carbon with improved mesoporous texture derived from biomass for enhanced adsorption of industrial cationic dye contaminants, *Mater. Chem. Phys.*, 282, 125881.

[21] Aljeboree, A.M., Alshirifi, A.N., and Alkaim, A.F., 2017, Kinetics and equilibrium study for the adsorption of textile dyes on coconut shell activated carbon, *Arabian J. Chem.*, 10, S3381–S3393.

[22] Medhat, A., El-Maghrabi, H.H., Abdelghany, A., Abdel Menem, N.M., Raynaud, P., Moustafa, Y.M., Elsayed, M.A., and Nada, A.A., 2021, Efficiently activated carbons from corn cob for methylene blue adsorption, *Appl. Surf. Sci. Adv.*, 3, 100037.

[23] Hajialigol, S., and Masoum, S., 2019, Optimization of biosorption potential of nano biomass derived from walnut shell for the removal of Malachite Green from liquids solution: Experimental design approaches, *J. Mol. Liq.*, 286, 110904.

[24] Subramanyam, B., and Das, A., 2014, Linearised and non-linearised isotherm models optimization analysis by error functions and statistical means, *J. Environ. Health Sci. Eng.*, 12 (1), 92.

[25] Bonilla-Petriciolet, A., Mendoza-Castillo, D.I., and Reynel-Ávila, H.E., 2017, *Adsorption Processes for Water Treatment and Purification*, Springer Cham, Switzerland.

[26] Prasad, A.L., Santhi, T., and Manonmani, S., 2015, Recent developments in preparation of activated carbons by microwave: Study of residual errors, *Arabian J. Chem.*, 8 (3), 343–354.

[27] Soldatkina, L., and Yanar, M., 2021, Equilibrium, kinetic, and thermodynamic studies of cationic dyes adsorption on corn stalks modified by citric acid, *Colloids Interfaces*, 5 (4), 52.

[28] Hien Tran, T., Le, A.H., Pham, T.H., Duong, L.D., Nguyen, X.C., Nadda, A.K., Chang, S.W., Chung, W.J., Nguyen, D.D., and Nguyen, D.T., 2022, A sustainable, low-cost carbonaceous hydrochar adsorbent for methylene blue adsorption derived from corncobs, *Environ. Res.*, 212, 113178.

[29] Ellerie, J.R., Apul, O.G., Karanfil, T., and Ladner, D.A., 2013, Comparing graphene, carbon nanotubes, and superfine powdered activated carbon as adsorptive coating materials for microfiltration membranes, *J. Hazard. Mater.*, 261, 91–98.

[30] Partlan, E., Davis, K., Ren, Y., Apul, O.G., Mefford, O.T., Karanfil, T., and Ladner, D.A., 2016, Effect of bead milling on chemical and physical characteristics of activated carbons pulverized to superfine sizes, *Water Res.*, 89, 161–170.

[31] Ando, N., Matsui, Y., Kurotobi, R., Nakano, Y., Matsushita, T., and Ohno, K., 2010, Comparison of natural organic matter adsorption capacities of super-powdered activated carbon and powdered activated carbon, *Water Res.*, 44 (14), 4127–4136.

[32] Ragadhita, R., and Nandiyanto, A.B.D., 2021, How to calculate adsorption isotherms of particles using two-parameter monolayer adsorption models and equations, *Indones. J. Sci. Technol.*, 6 (1), 205–234.

[33] Agbovi, H.K., and Wilson, L.D., 2021, "Adsorption Processes in Biopolymer Systems: Fundamentals to Practical Applications" in *Natural Polymers-Based Green Adsorbents for Water Treatment*, Eds. Kalia, S., Elsevier, Cambridge, US, 1–51.

[34] Yao, C., and Chen, T., 2017, A film-diffusion-based adsorption kinetic equation and its application, *Chem. Eng. Res. Des.*, 119, 87–92.

[35] Sreńscek-Nazzal, J., Narkiewicz, U., Morawski, A.W., Wróbel, R.J., and Michalkiewicz, B., 2015, Comparison of optimized isotherm models and error functions for carbon dioxide adsorption on activated carbon, *J. Chem. Eng. Data*, 60 (11), 3148–3158.

[36] Nandiyanto, A.B.D., Oktiani, R., and Ragadhita, R., 2019, How to read and interpret FTIR spectroscope of organic material, *Indones. J. Sci. Technol.*, 4 (1), 97–118.

[37] Jawad, A.H., Saud Abdulhameed, A., Wilson, L.D., Syed-Hassan, S.S.A., ALOthman, Z.A., and Rizwan Khan, M., 2021, High surface area and mesoporous activated carbon from KOH-activated dragon fruit peels for methylene blue dye adsorption: Optimization and mechanism study, *Chin. J. Chem. Eng.*, 32, 281–290.